JBC ARTICLE

# A dynamic anchor domain in slc13 transporters controls metabolite transport

Received for publication, September 4, 2019, and in revised form, February 26, 2020 Published, Papers in Press, March 9, 2020, DOI 10.1074/jbc.RA119.010911

**Ahlam Khamaysi, Sara Aharon, Hadar Eini-Rider, and Ehud Ohana**[1]

*From the Department of Clinical Biochemistry and Pharmacology, Faculty of Health Sciences, Ben-Gurion University of the Negev, Beer-Sheva 8410501, Israel*

Edited by Jeffrey E. Pessin

**Metabolite transport across cellular membranes is required for bioenergetic processes and metabolic signaling. The solute carrier family 13 (slc13) transporters mediate transport of the metabolites succinate and citrate and hence are of paramount physiological importance. Nevertheless, the mechanisms of slc13 transport and regulation are poorly understood. Here, a dynamic structural slc13 model suggested that an interfacial helix, H4c, which is common to all slc13s, stabilizes the stationary scaffold domain by anchoring it to the membrane, thereby facilitating movement of the SLC13 catalytic domain. Moreover, we found that intracellular determinants interact with the H4c anchor domain to modulate transport. This dual function is achieved by basic residues that alternately face either the membrane phospholipids or the intracellular milieu. This mechanism was supported by several experimental findings obtained using biochemical methods, electrophysiological measurements in *Xenopus* oocytes, and fluorescent microscopy of mammalian cells. First, a positively charged and highly conserved H4c residue, $Arg^{108}$, was indispensable and crucial for metabolite transport. Furthermore, neutralization of other H4c basic residues inhibited slc13 transport function, thus mimicking the inhibitory effect of the slc13 inhibitor, slc26a6. Our findings suggest that the positive charge distribution across H4c domain controls slc13 transporter function and is utilized by slc13-interacting proteins in the regulation of metabolite transport.**

The major succinate and citrate transporters expressed on the plasma membrane of mammalian cells are members of the slc13 family (1–3), which is part of the larger divalent anion: sodium symporter family (4). The physiological importance of slc13 transporters and, among them, the citrate transporter slc13a5 (NaCT), is underscored by numerous pathologies that are associated with these genes including hypertension, kidney stones, and epilepsy (5–8). Being the major citrate transporter, NaCT deletion mimics caloric restriction, which promotes prolonged life span in *Drosophila melanogaster* (9). In mice, several metabolic changes including elevated energy expenditure and reduced lipogenesis protect $NaCT^{-/-}$ mice from adiposity and insulin resistance (10).

Interaction between the oxalate transporter and the succinate/citrate transporter results in inhibition of succinate transport (6, 7) and is associated with protection from kidney stone formation and hypertension (6, 7). However, the molecular mechanism that mediates the interaction with slc13 transporters to regulate their activity is unknown. Notably, the crystal structure of the bacterial slc13 homolog, vcINDY, reveals structural determinants in detail identifying the substrate-binding sites and potential conformational changes that facilitate ion movement (12, 13). Putative models of the mammalian transporters describe an elevator-type transport kinetics showing that the entire ion-binding site moves through the lipid barrier, and thus, the substrates are alternately exposed to both sides of the membrane (14). Structural analyses suggest that slc13 transporters have a dimeric structure and that each protomer consists of 11 transmembrane domains (TMDs).[2] TMDs 3, 4, 8, and 9 form the interface between the two protomers. TMDs 4, 5, 9, and 10 are different from other TMDs because they are "broken" to several helices within the membrane that do not fully span the membrane bilayer. Specifically, TMD 4 consists of three segments, two of which, 4a and 4b, are involved in forming the dimerization interface, whereas the third segment, TM 4c or the H4c domain, is located near the surface of the inner membrane. We have previously reported that the putative H4c domain of the slc13 family member, NaDC-1, mediates interaction with partner proteins (6, 7). We showed that a positively charged residue, $Lys^{107}$, on the H4c domain of NaDC-1 mediates interaction with a Glu residue ($Glu^{613}$) in the intracellular C-terminal domain (STAS domain) of slc26 transporters. Thus, the binding and regulation of NaDC-1 are facilitated by charged residues. It is therefore plausible that charged moieties of H4c play a key role in slc13 transporters regulation through electrostatic interactions. In numerous proteins, helices that are found in the membrane-cytoplasm interface, like H4c, are buried in the hydrophobic milieu, while extending the side chain of positively charged basic residues to the polar environment in a process termed "snorkeling" (15–17). The snorkeling is required for anchoring membrane proteins to the membrane and for protein stabilization. Here, we asked how does the charge distribution across the H4c domain affect slc13-mediated transport? Because H4c appears to be a pivotal

This work was supported by United States–Israel Binational Science Foundation Grant 2015003 (to E. O.) and by Israel Science Foundation Grants 271/16 and 2164/16 (to E. O.). The authors declare that they have no conflicts of interest with the contents of this article.

This article contains Movie S1 and Figs. S1–S4.

[1] To whom correspondence should be addressed: Dept. of Clinical Biochemistry and Pharmacology, Faculty of Health Sciences, Ben-Gurion University of the Negev, Beer-Sheva 8410501, Israel. E-mail: ohanaeh@bgu.ac.il.

[2] The abbreviations used are: TMD, transmembrane domain; MD, molecular dynamics; CoIP, co-immunoprecipitation.

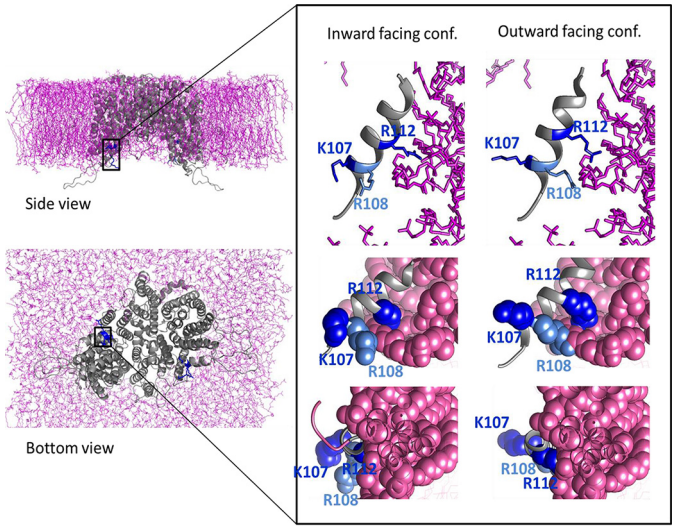


**Figure 1. The putative SLC13A5 model based on the vcINDY crystal structure, MD analysis of membrane lipid interaction, and computational optimization of membrane protein structure in lipid bilayer.** Side and bottom views of the hNaCT model embedded within the lipid bilayer are shown. The *inset* shows the H4c helix and the three basic residues $Lys^{107}$, $Arg^{108}$, and $Arg^{112}$ in the inward- and outward-facing conformations (*conf.*) as indicated. Note that $Lys^{107}$ faces the intracellular region, whereas $Arg^{108}$ and $Arg^{112}$ interact with the membrane lipids.

structural junction that receives inputs from several determinants because of its interaction with the membrane, intracellular proteins, and the slc13 catalytic domain, it may be quintessential for controlling cellular metabolite transport and homeostasis, which is mostly unknown.

## Results

### *The orientation of putative slc13-H4c basic residues is dynamically altered*

To study the role that the positive residues play in slc13 transport kinetics, we utilized homology modeling to generate a putative structure of human NaCT embedded within the membrane based on the crystal structure and molecular dynamics analysis of vcINDY (Fig. 1). Our analysis suggests that $Arg^{108}$ and $Arg^{112}$ have similar orientation because they are separated by a full helical turn. Therefore, both residues potentially interact with the phospholipids. In addition, the $Lys^{107}$ faces the intracellular milieu, based on this analysis. Importantly, the inward- and outward-facing models of hNaCT suggest that $Lys^{107}$ and $Arg^{112}$ are oriented in opposite directions and have limited movement, whereas in contrast, $Arg^{108}$ rotates to alternately interact with the phospholipids or intracellular components. Our *in silico* analysis indicates that $Arg^{108}$ may have a pivotal role in both stabilizing the interaction with the membrane phospholipids and interaction with other proteins, whereas the positive charge distribution and dynamics of $Lys^{107}$ and $Arg^{112}$ may support or restrict $Arg^{108}$ to facilitate slc13 function.

### *The highly conserved slc13-H4c ($Arg^{108}$) residue is indispensable for slc13 function*

To study the role that each of the positive residues plays in slc13 function, we performed multiple sequence alignment (Fig. 2*A*) and utilized the Consurf software (18) (Fig. 2*B*). The results indicated that $Arg^{108}$ is a highly conserved residue (score 9) and is practically irreplaceable in plants, flies, mammals, and even specific bacteria. $Lys^{107}$ is also conserved but with a lower conservation score (score 8), whereas $Arg^{112}$ received the lowest score of the three positively charged residues (score 3). These findings together with the unique putative kinetics depicted in Fig. 1 suggest that $Arg^{108}$ may be crucial for the function or regulation of slc13 transporters. To test the functional role of this residue, we mutated $Arg^{108}$ in NaDC-1 to alanine (R108A) and monitored succinate currents in *Xenopus* oocytes. The function of NaDC-1(R108A) was completely abolished (Fig. 2*C*).

To study the general role of H4c in the slc13 family, we utilized the putative hNaCT (SLC13A5) model (Fig. 1 and Fig. S1), which has similar positive charges in the same locations as NaDC-1 (SLC13A2). We have generated three different $Arg^{108}$ mutations, namely, R108A that neutralizes the charge, R108K that preserves the charge, and R108D that swaps the charge from positive to negative. We monitored citrate-dependent currents in *Xenopus* oocytes injected with different human NaCT cRNA, which were held at −60 mV. As indicated in Fig. 3*A*, all hNaCT $Arg^{108}$ mutations largely abolished citrate currents. Moreover, we found that the hNaCT(K107R/R108K), which retains the positive charge but swaps the Lys and Arg at these adjacent positions, does not recover hNacT function. To decipher the effect of $Lys^{107}$ and $Arg^{112}$ on transport, we monitored the function of the double mutant hNaCT(K107A/R112A). The results in Fig. 3*B* indicate that although attenuated, a significant residual activity (50% of WT) existed in the double mutant. These results indicate that transport activity can be maintained by $Arg^{108}$ as the sole basic residue of the H4c domain, even in the absence of the two adjacent positively charged residues. The H4c domain is essential for protein–protein interactions between NaDC-1 and slc26a6, which inhibits transport of succinate by NaDC-1. We have previously shown that slc26a6($Glu^{613}$) is involved in mediating interaction with NaDC-1 (6, 7). Here, we found that the slc26a6(E613A) does not inhibit NaCT (Fig. 3*B*) and impairs the interaction with NaCT (Fig. 3*C*). We therefore functionally challenged the role of $Lys^{107}$ and $Arg^{112}$ in this interaction. We monitored the function of either hNaCT or hNaCT(K107A/R112A) in the presence or absence of slc26a6. We found that both hNaCT and hNaCT(K107A/R112A) are significantly inhibited by slc26a6, suggesting that when both residues are mutated, the interaction between NaCT and slc26a6 is preserved (Fig. 3*B*). The major role of $Arg^{108}$ in regulating transport activity may suggest that this residue alone, in the absence of the charge on $Lys^{107}$ and $Arg^{112}$, can support transport activity and the interaction with slc26a6.

To investigate how the basic amino acids of the H4c domain affect hNaCT binding to slc26a6, we monitored human and mouse slc26a6 interaction with either hNaCT(WT), the functional hNaCT(K107A) mutant, and the dysfunctional hNaCT(R108A), hNaCT(R108D) mutants by CoIP. The input protein levels were adjusted to detect changes in CoIP. As control, we also monitored the interaction between hNaCT and mA6(E613A), which showed lower interaction with hNaCT (Fig. 3*C*) in agreement with previous results (6). The results

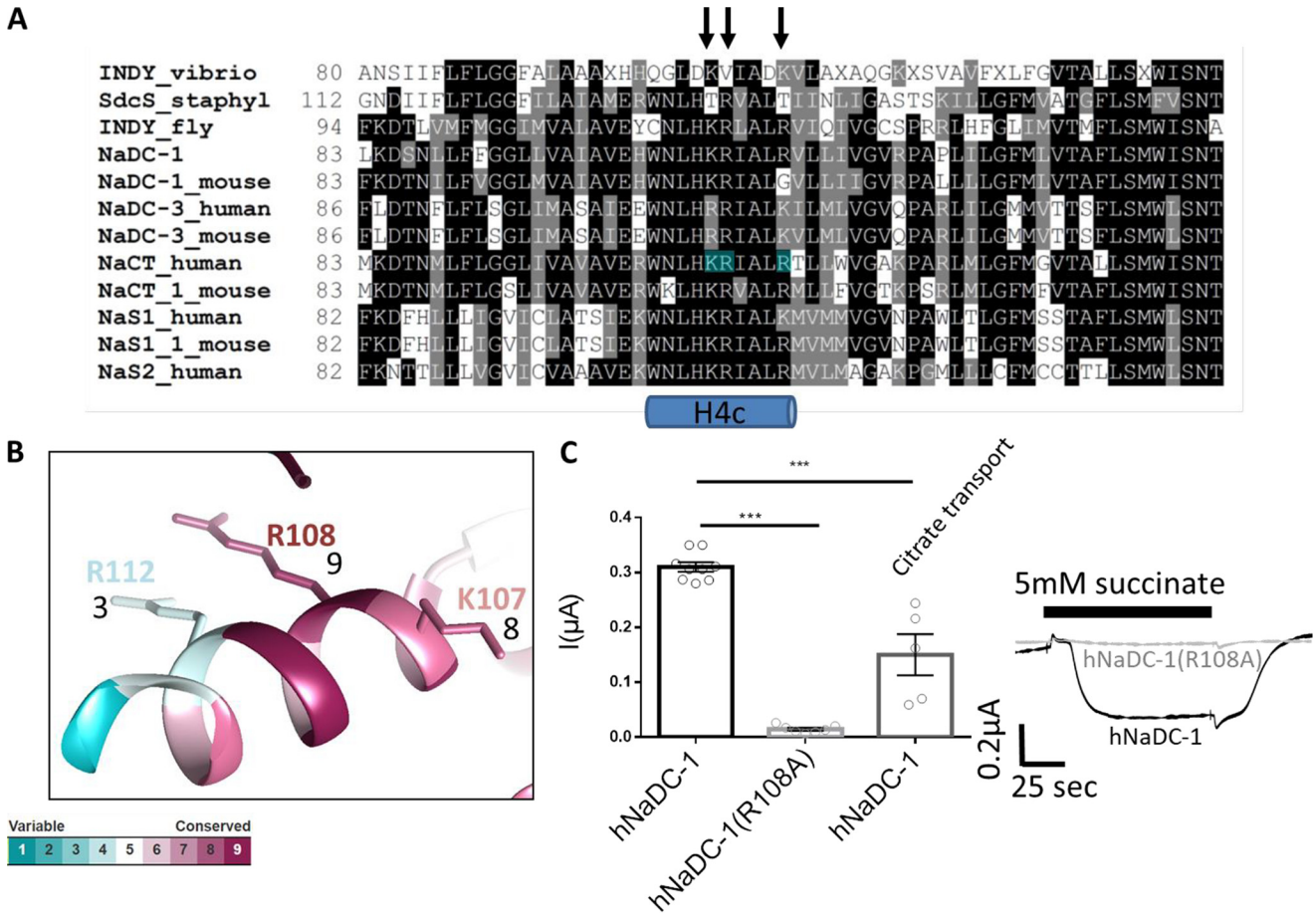


**Figure 2. The H4c positively charged residues are conserved.** *A*, the sequences of several bacterial, fly, and mammalian slc13 homologs were analyzed using ClustalW (29). The three basic H4c residues are indicated by *black arrows* and highlighted in *cyan* for the human NaCT sequence. *B*, 3D representation of the H4c helix conservation color codes based on the Consurf software analysis. The residues and their respective conservation scores are indicated. *C*, summary and representative traces of hNaDC-1-dependent $Na^+$ succinate current in *Xenopus* oocytes expressing WT hNaDC-1 or hNaDC-1(R108A). We also monitored hNaDC-1–dependent $Na^+$ citrate currents (citrate transport) showing lower citrate currents because of lower selectivity for citrate, as previously reported.

in Fig. 3 (*C* and *D*) further show that both human and mouse slc26a6 interaction with $Lys^{107}$ and $Arg^{108}$ mutants is significantly reduced compared with the binding with hNaCT(WT). This indicates that $Lys^{107}$ and $Arg^{108}$ mutations interfere with slc26a6 binding, regardless of whether the mutant abolishes hNaCT activity or not. Therefore, the basic amino acids of the H4c domain either mediate interaction with slc26a6-STAS domain residues directly or maintain H4c helix stability that is essential for this interaction. Furthermore, the dysfunction of several mutations that we have identified could be a result of impaired trafficking to the membrane. Hence, we monitored membrane expression in mammalian cells using a biotinylation assay (Fig. 3*E*) and cellular distribution by fluorescent immunocytochemistry (Fig. S2). As suggested by the summary and statistical analysis in Fig. 3*E*, the membrane expression of the inactive mutants R108D, K107D, R108K, R112D, and R108A was not reduced compared with WT. This suggests that hampered mutant $Arg^{108}$ protein function is not caused by impaired trafficking to the membrane but rather by impairment of protein kinetics.

Because the three $Arg^{108}$ mutants retained only a very low activity compared with WT, we assessed whether their activity could be induced by different membrane potentials. Therefore, *I–V* curves for $Arg^{108}$ mutants were obtained (see "Experimental procedures"; Fig. 3, *F* and *G*). Conductance was calculated as the slope of linear fit to the *I–V* curves (Fig. 3*H*), and the results indicate that hNaCT conductance is dramatically reduced but maintained in all $Arg^{108}$ mutants. Moreover, the residual conductance is charge-dependent: highest conductance for positive Lys charge (R108K), reduced conductance for neutral Ala residue (R108A), and lowest conductance for the negative (R108D). This suggests that the charge of $Arg^{108}$ is critically regulating the transport of citrate via hNaCT. The very low transport activity of all $Arg^{108}$ mutants at all membrane potentials is in agreement with our *in silico* analyses (Fig. 1), which predicts that $Arg^{108}$ is quintessential for slc13 function and is irreplaceable.

### *The H4c-$Lys^{107}$ residue is required to maintain full slc13 activity and regulation*

Remarkably, we have previously shown that a single mutation that neutralizes the charge on NaDC-1($Lys^{107}$) abolished the interaction with slc26a6 and therefore the inhibition of succinate transport (6, 7). We therefore asked whether $Lys^{107}$ mutants of hNaCT would also impair the interaction with slc26a6. Hence, we monitored the citrate transport activity

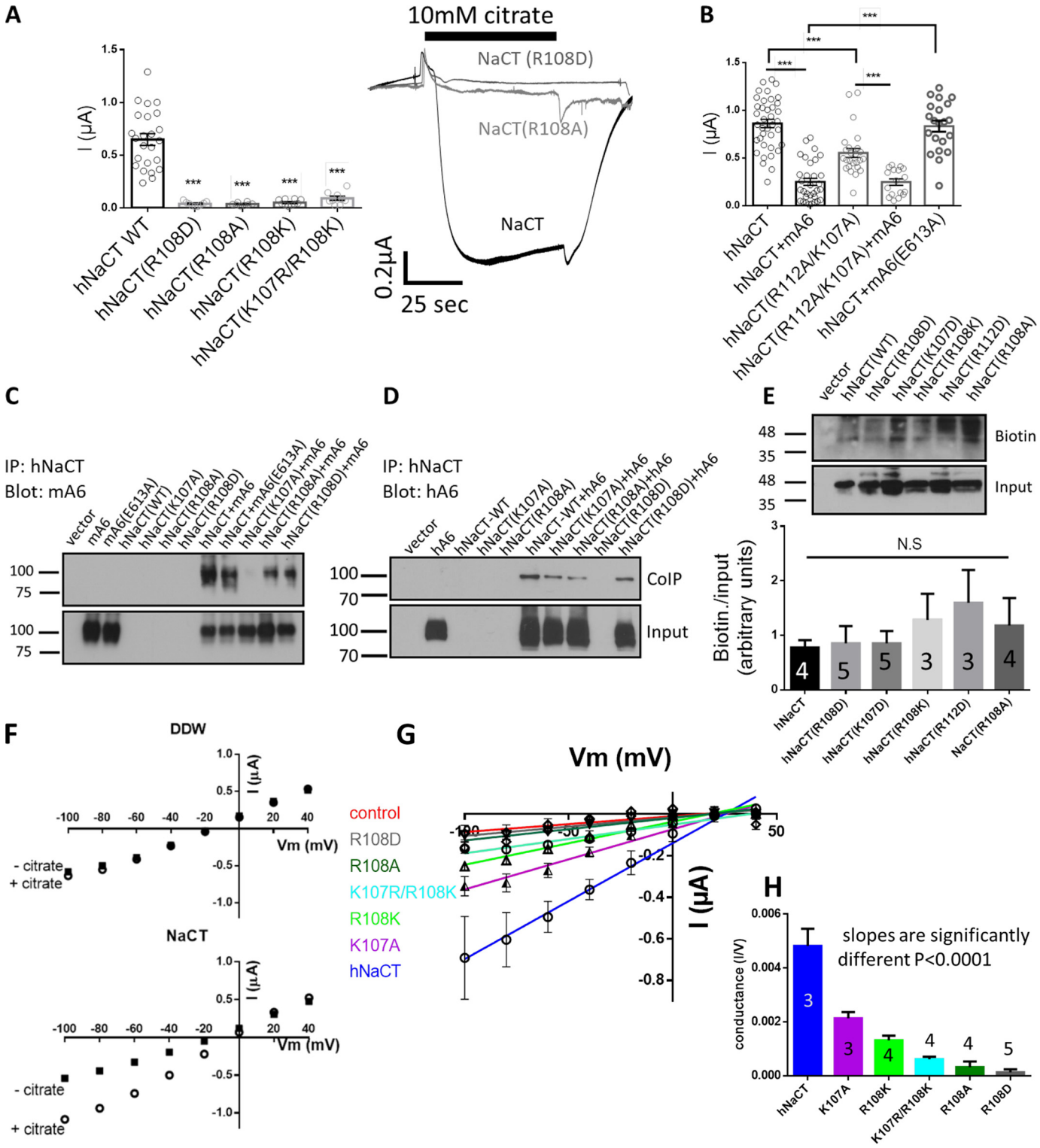


**Figure 3. The highly conserved Arg$^{108}$ is crucial for slc13 function and irreplaceable.** *A*, summary and representative traces of hNaCT-dependent $Na^+$ citrate current in *Xenopus* oocytes expressing hNaCT(WT) or different hNaCT(Arg$^{108}$) mutations. *B*, summary of hNaCT-dependent $Na^+$ citrate current of hNaCT(K107A/R112A) double mutant in the absence or presence of slc26a6 compared with hNaCT(WT) alone or hNaCT and the mA6(E613A) mutant. *C* and *D*, the interaction between hNaCT mutants and either mouse (mA6) or human (hA6) slc26a6 were monitored by CoIP analysis as indicated in *C* and *D*, respectively. *E*, Western blotting analysis and summary of the indicated hNaCT mutations membrane expression monitored using biotinylation assay is shown. *F*, *I–V* curves of individual experiments of *Xenopus* oocytes that were injected with either double-distilled water (*DDW*) as negative control or with human NaCT. Next, the cells were perfused with a $Na^+$-containing solution in the absence (−*citrate*) or presence (+*citrate*) of 10 mM citrate. *G*, the base-line currents calculated by subtracting the citrate currents from background (−*citrate*). *H*, conductance was calculated as the slopes of linear fit to the *curves* in *G* ($p < 0.0001$). *IP*, immunoprecipitation; *N.S*, not significant.

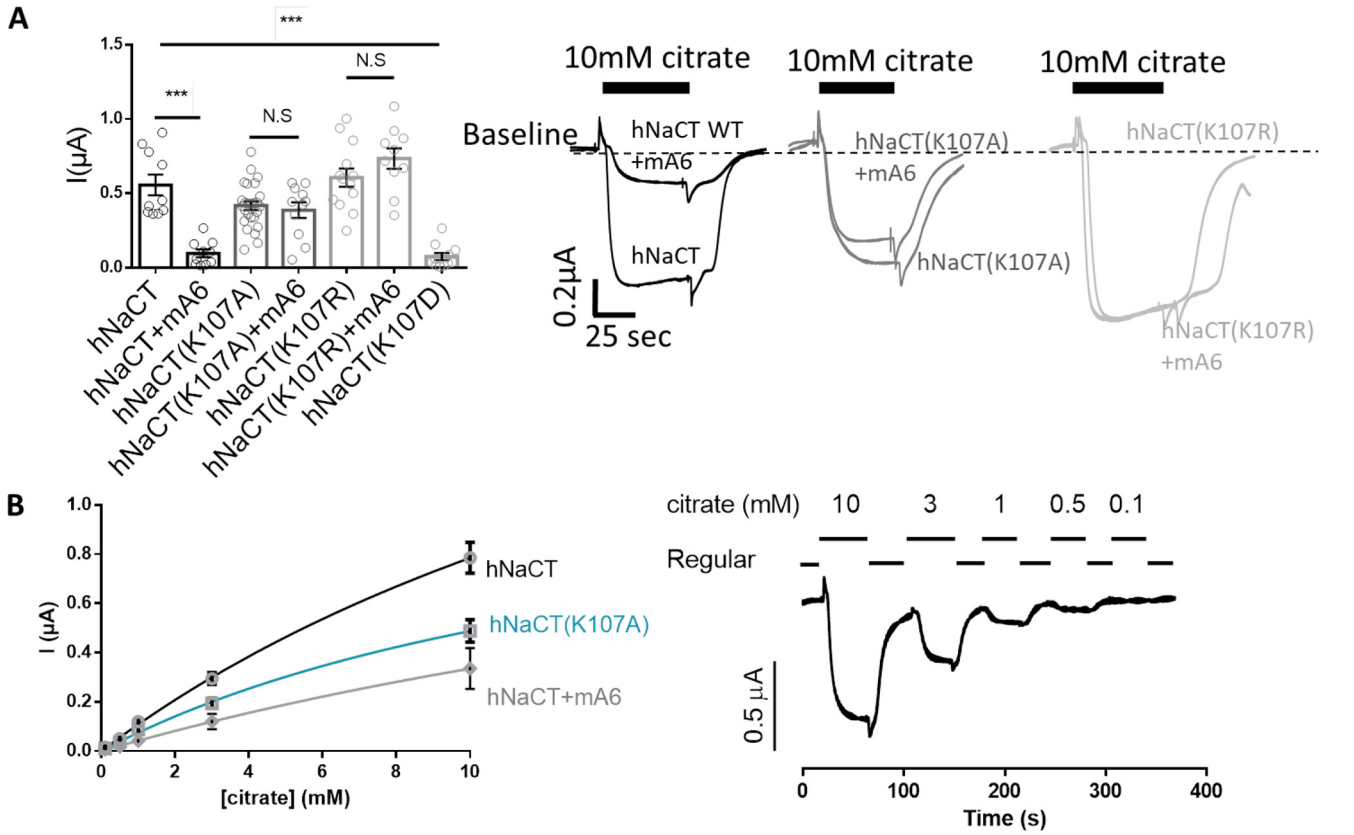


**Figure 4. hNaCT Lys$^{107}$ regulates citrate transport and K107A mutant mimics interaction with slc26a6.** *A*, summary and representative traces of hNaCT-dependent $Na^+$ citrate current in *Xenopus* oocytes expressing hNaCT(WT) or hNaCT(Lys$^{107}$) mutants with or without slc26a6. *B*, dose-dependent NaCT-mediated citrate currents monitored in oocytes expressing hNaCT(WT), hNaCT(K107A), or hNaCT + mA6. The sample traces in *B* were monitored for hNaCT(WT). *N.S*, not significant.

of K107A, K107R, or K107D in the presence or absence of slc26a6 as shown in Fig. 4*A*. Our results indicated that the hNaCT(K107A) was partially active and the hNaCT(K107R) activity was fully retained. Although hNaCT(K107A) activity is lower than hNaCT, the residual function is unaffected by slc26a6, whereas hNaCT is largely inhibited by slc26a6. Moreover, the hNaCT(K107R) that fully preserved transport activity is also slc26a6-independent. In contrast, the presence of the single mutant K107D abolished hNaCT function altogether, similar to the effect of R108D mutant. Finally, to determine whether Lys$^{107}$ regulates the transport kinetics, we performed a dose-response measurement of hNaCT-mediated citrate transport in cells expressing either hNaCT(K107A) mutant or hNaCT in the presence of slc26a6. As shown in Fig. 4*B*, hNaCT(K107A) mutant mimics the inhibitory effect of slc26a6 on hNaCT transport kinetics. We show that although the positive charge at location 107 is not crucial to retain transport, in contrast to Arg$^{108}$, Lys$^{107}$ is necessary for regulation by slc26a6. However, in the absence of a positive charge at position 112, the role of Lys$^{107}$ in binding and regulation of hNaCT by slc26a6 is negligible, because hNaCT(K107A/R112A) inhibition by slc26a6 is rescued. Together, these findings suggest that Lys$^{107}$ supports Arg$^{108}$ to achieve maximal transport function. Moreover, the Lys$^{107}$ residue is crucial for the regulation of hNaCT by slc26a6, as previously shown for NaDC-1 where Lys$^{107}$ mediates the interaction with slc26a6-STAS domain (6, 7).

### *The functional role of H4c-Arg$^{112}$ residue is similar to H4c-Lys$^{107}$*

Our putative slc13 model (Fig. 1) shows that Arg$^{112}$ is oriented similarly to Arg$^{108}$. Nonetheless, Arg$^{112}$ is far less conserved than Arg$^{108}$, and the predicted outward-facing model of hNaCT indicates that, unlike Arg$^{108}$, the Arg$^{112}$ residue rotation does not significantly change its spatial orientation (Fig. 1). To determine the role of Arg$^{112}$ in hNaCT transport and interaction with the regulatory slc26a6, we monitored citrate transport by different Arg$^{112}$ mutations. Specifically, R112A and R112K retained activity yet abolished regulation by slc26a6, whereas R112D activity was dramatically reduced (Fig. 5). These findings suggest a similar role for Lys$^{107}$ and Arg$^{112}$ in regulating hNaCT transport and interaction with slc26a6. Furthermore, these results underscore the quintessential function of Arg$^{108}$ that preserves hNaCT function and rescues regulation by slc26a6 in the absence of positive charge at both positions 107 and 112.

## Discussion

Numerous studies that investigated the transport of metabolites across cell membranes revealed noncanonical metabolic pathways that are essential for cellular function and the impairment of which results in severe pathologies. Specifically, impaired $Na^+$-dependent metabolite transport was implicated with metabolic pathologies, high morbidity, and high mortality

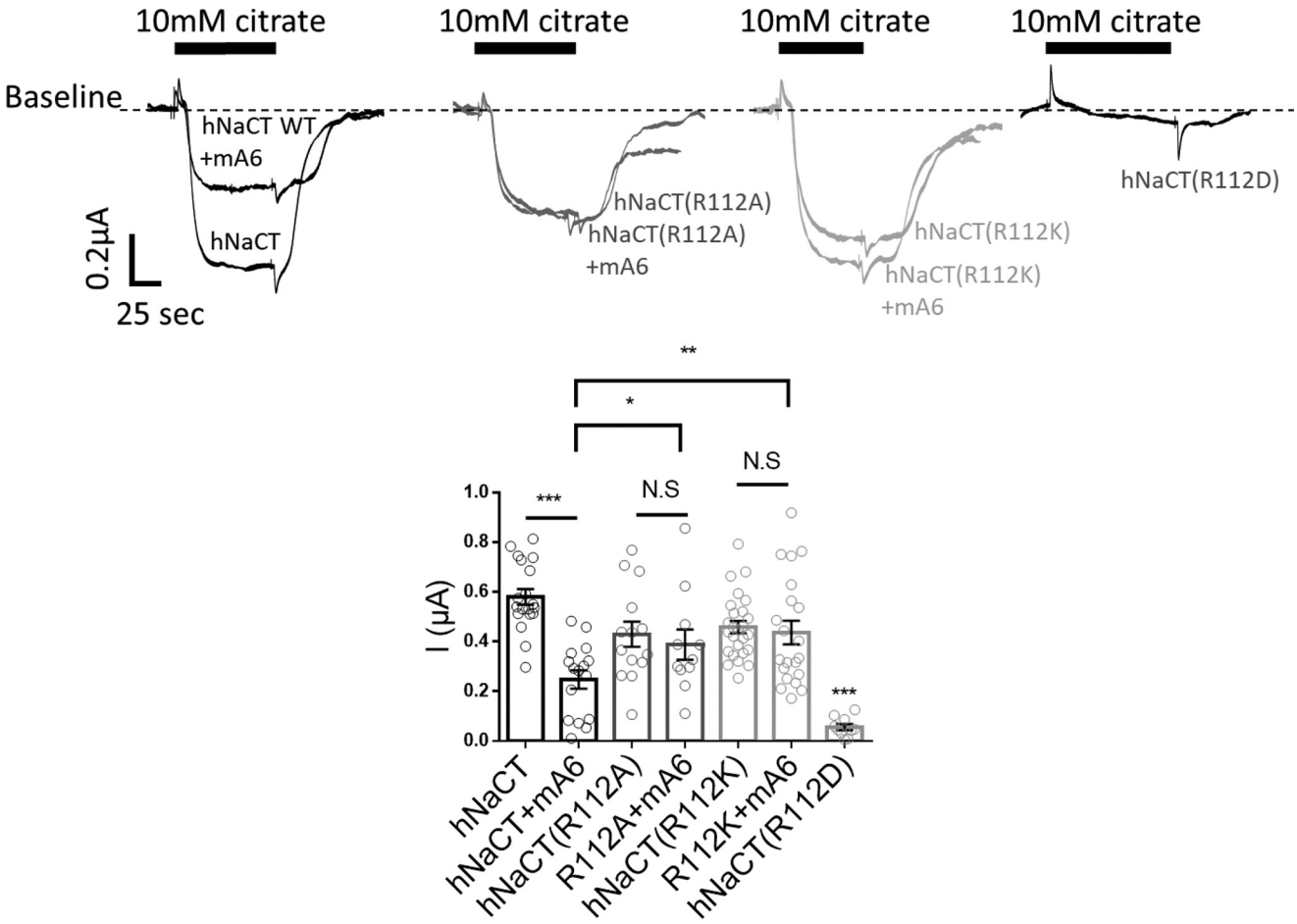


**Figure 5. NaCT Arg$^{112}$ regulates citrate transport and affects interaction with slc26a6 similarly to Lys$^{107}$.** Summary and representative traces of hNaCT-dependent $Na^+$ citrate current in *Xenopus* oocytes expressing hNaCT(WT) or hNaCT(Arg$^{112}$) mutants with or without slc26a6 (mA6) are shown. *N.S*, not significant.

diseases. The most prominent example is the $Na^+$-dependent glucose transporter family (SGLT). The cloning of the first SGLT more than 30 years ago made a significant impact in the field of glucose metabolism (19). Impaired SGLT function has been associated with type II diabetes, early pregnancy failure, glucose–galactose malabsorption, and familial renal glucosuria (20). It is therefore not surprising that SGLTs are currently major therapeutic targets for type II diabetes because SGLT inhibitors efficiently inhibit glucose absorption, thus lowering blood sugar.

The transport of key TCA cycle metabolites such as succinate and citrate by slc13 transporters is expected to modulate cellular metabolism and bioenergetics. In the mouse liver, knockout of the slc13 transporter, NaCT, inhibits lipogenesis by lowering the cytoplasmic concentrations of the fatty acid biogenesis intermediate: citrate (10). However, functional human NaCT measurements in *Xenopus* oocytes show significantly lower affinity to citrate compared with the reported mouse isoform, as we report here and previously reported by Zwart *et al.* (22). When monitored in mammalian cells, human NaCT $K_m$ was ~600 $\mu$M (23). These differences between human and mouse isoforms may be attributed to diverse regulatory mechanisms or metabolic requirements. In addition, human cells express at least three additional splice variants, which were not carefully tested. Further studies are required to understand the role of NaCT function and regulation in human metabolism. In the immune system, cytoplasmic succinate and citrate are emerging as pivotal metabolic regulators of inflammation in macrophages and dendritic cells (24, 25). In the kidney, impaired slc13-mediated reabsorption of succinate and citrate results in kidney stone formation and hypertension, as shown in mice (6, 7). These studies suggest that more knowledge of the regulation mechanisms of slc13 transporters is required to understand the physiological function of succinate and citrate.

As we have previously shown, the H4c domain of slc13s mediates intracellular interaction with slc26a6, which results in inhibition of two slc13 transporters, NaDC-1 and, as we show in the current study, hNaCT (6). The functional and *in silico* analyses of mutations in H4c basic residues suggest that Arg$^{108}$ is essential because of its positive charge and other exclusive attributes such as the hydrophilicity, size, and optional rotamers of the residue. However, Lys$^{107}$ and Arg$^{112}$ are required for protein–interaction and hNaCT regulation. A negative charge at locations 107 and 112 most likely neutralizes Arg$^{108}$ and is expected to abolish transport, as indeed occurs for K107D and R112D but not with other mutants (Figs. 4*A* and 5). This indicates that the positive charge distribution in H4c is achieved by

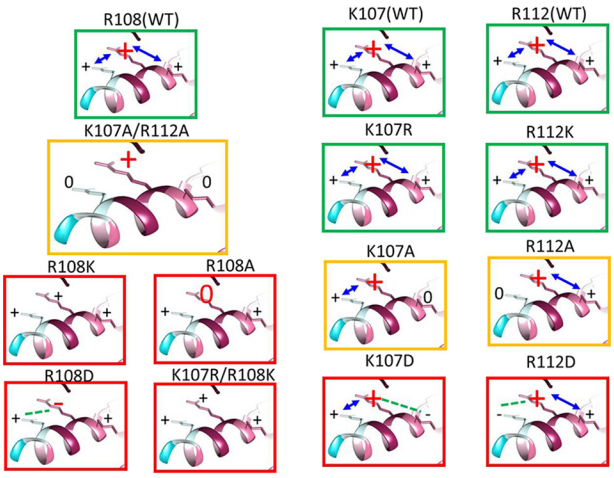


**Figure 6. A model of H4c charged residues regulation of NaCT function.** Each *box* depicts the charge distribution of H4c for each mutation. Dysfunctional mutations, functional mutations, and mutations with attenuated function are indicated by *red*, *green*, and *yellow boxes*, respectively. The only mutation that retains regulation by slc26a6 is K107A/R112A double mutation. The model suggests that when the pivotal $Arg^{108}$ charge is hampered by either $Arg^{108}$ mutations or negative charge in proximal basic residues, then hNaCT function is abolished, whereas $Lys^{107}$ and $Arg^{112}$ are necessary but not crucial to retain function.

all three positive residues; it is required for maximal hNaCT activity and is essential for regulation by slc26a6. However, the only H4c basic residue that is absolutely essential to maintain transport function is $Arg^{108}$ because the Arg in this position is indispensable. When $Lys^{107}$ and $Arg^{112}$ charge is neutralized, hNaCT function is inhibited but not abolished because the $Arg^{108}$ charge remains unaffected, yet the overall H4c net charge is reduced (Fig. 6). In addition, the H4c positive charge distribution is critical for interaction with the slc26a6 protein. Indeed, all hNaCT single mutations retained activity but impaired the interaction with and regulation by slc26a6, except for the K107A/R112A double mutant, which is inhibited by slc26a6. This shows that slc13 transporter function is inhibited by dissipating the positive charge of H4c either by mutations or through interaction with slc26a6. Thus, the underlying mechanism of slc26a6 regulation of the slc13 transporters activity is likely via dissipation of the H4c domain-positive charge. Because we utilize site-directed mutations to study NaCT function, it is plausible that specific mutants have affected H4c structure. However, this can be resolved only by future structural analysis.

A key question that stems from our findings is how does the H4c charge distribution affect slc13 transporter kinetics? One plausible explanation is that reduced positive charge in H4c impairs the stability of its position relative to the membrane because of either changes in the stability of the helical fold, interaction with the membrane, or both. Based on the kinetic model of the slc13 homolog, vcINDY, the $HP_{in}$ domain within the transport domain of vcINDY makes a considerable movement during every turnover cycle (14). Our *in silico* analysis suggests that hydrophobic residues of the H4c domain interact with hydrophobic residues of $HP_{in}$. Therefore, the hydrophobic interactions between the stationary H4c and the highly mobile $HP_{in}$, which participates in ligand binding, are potentially essential for the movement of the entire transport domain and may provide the mechanistic answer as to how H4c affects slc13 transport. Furthermore, the H4c helix is partially embedded within the membrane inner leaflet, and it has three basic residues rotated in different directions relative to the polar/nonpolar inner membrane surface. During every turnover cycle, $Arg^{108}$ alternately rotates between the polar and nonpolar environments (snorkeling), whereas $Lys^{107}$ and $Arg^{112}$ rotation does not change their general orientation (Fig. S3). In agreement with this model, our functional data suggest that $Arg^{108}$ is indeed indispensable. However, why do $Lys^{107}$ and $Arg^{112}$ show similar functional and regulatory patterns, although they have opposite orientation in the inward-facing conformation? We reason that these residues support or confine $Arg^{108}$ rotation, depending on whether it interacts with the membrane (like $Arg^{112}$) or rotates toward the intracellular milieu (like $Lys^{107}$). To prove this mechanism of slc13 transport and regulation, further molecular dynamics and structural analyses are required.

The vcINDY inward- and outward-facing conformations and our putative hNaCT model show that the loop (Fig. S4) that connects H4c to $HP_{in}$ is highly flexible. The loop flexibility is achieved by highly conserved Gly and Pro residues that are predicted to form a "hinge" structure that enables wide-range rotation. Hence, a stable H4c domain on one hand and a flexible hinge on the other facilitate the "elevator" movement of the transport domain to efficiently transport ions. Thus, reduced stability of the H4c position relative to the membrane is expected to hamper transport efficiency resulting in slc13 transport inhibition. Altogether, our results delineate the mechanism by which the charge distribution on the H4c domain on slc13 transporters controls cellular metabolite transport.

## Experimental procedures

### *Animal care*

All the work on *Xenopus laevis* was approved by the Institutional Animal Care and Use Committee of the Ben Gurion University of the Negev.

### *3D protein model prediction and multiple sequence alignment*

The putative structure of hNaCT was predicted using HHPred software (26) with high homology to the crystal structure of a bacterial dicarboxylate/sodium symporter (Protein Data Bank code 5UL9). Prediction parameters were as follows: probability = 100, *E* value = 5.4e-30, score = 273.56, identities = 30%, similarity = 0.49, secondary structure score = 54.8, matched columns = 440, and length = 445. The membrane-embedded model was generated based on the molecular dynamics (MD) simulation of 5UL9 from memprotMD database (27). To generate the dynamic model, the putative human NaCT structure was aligned to both the inward-facing vcINDY crystal structure and the outward-facing model (14). Both models were aligned to the inward-facing MD model. All final models and morph movies (Movies S1, *A–C*) were generated and visualized using UCSF Chimera 1.11 (28). Multiple sequence alignment was performed using ClustalW software (29).

### Plasmid construction, mutagenesis, and cRNA preparation

We used the human *NaDC-1* clone (NCBI accession no. BC096277) in the pCMV6-AC-Myc-His vector; the mouse *slc26a6* (NCBI accession no. NM_134420) in the pCMV6-AC-mKate vector; the human *slc26a6* (NCBI accession no. NM_022911) in the pCMV6-AC-mKate vector; and the human *NaCT* in pC4-TOPO (NCBI accession no. BC_104795). We subcloned the human *NaCT* into both pCMV6-AC-Myc-His and pCMV6-AC-mKate. All site-directed mutants were generated with QuikChange Lightning site-directed mutagenesis kit (Agilent, Santa Clara, CA). All constructs including the in-house generated site-specific mutants were verified by sequencing and immunoblot of the protein products. The genes in pC4-TOPO were linearized using relevant restriction enzymes and transcribed *in vitro* with T7 mMessage mMachine ultra (Thermo Fisher Scientific).

### Preparation and injection of oocytes

Oocytes were obtained by a partial ovariectomy of female *X. laevis* (*Xenopus* One, Dexter, MI), as previously described (30). Briefly, the frogs were anesthetized, and follicle cells were removed in an OR-2 calcium-free medium. The defolliculated oocytes were washed with OR-2 calcium-free medium, and healthy oocytes in stages V to VI were identified, collected under binoculars and maintained overnight at 18 °C in an ND96 solution. 32 nl of the different cRNA were injected into the oocytes using a Nanoliter 2010 injector (World Precision Instruments, Inc., Sarasota, FL). Similar volumes and concentrations (4 $\mu$g/$\mu$l) of cRNA or water were mixed to achieve similar amounts of injected cRNA per oocyte. The oocytes were incubated at 18 °C in an ND96 solution with pyruvate and antibiotics and were studied 48–96 h after cRNA injection. The use of several oocyte batches may result in functional variance as we observed. To overcome this technical obstacle, we monitored the currents in oocytes injected with either water or hNaCT(WT) in the absence or presence of slc26a6 and summarized the data for each batch.

### Voltage and current measurement in oocytes

Voltage and current recordings were performed with a two-electrode voltage clamp as described (7). The current was recorded with a Warner Instrument Corporation amplifier model OC-725C (Hamden, CT) and digitized via an A/D converter (Digidata 1550A; Axon Instruments, Inc.). The electrodes were backfilled with a 3 M KCl solution. During measurements, two channels were used to record and control the membrane potential. The data were analyzed using the Clampex 10 system (Axon Instruments, Inc.). The following solutions were used as indicated in the figures: standard HEPES-buffered ND96 oocyte regular medium containing 96 mM NaCl, 2 mM KCl, 1.8 mM $CaCl_2$, 1 mM $MgCl_2$, and 5 mM HEPES, pH 7.5. $Na^+$ citrate and $Na^+$ succinate were added to the solutions as indicated in the figures. The *I–V* curves were obtained before perfusion with a citrate-containing solution and subtracted from the curves obtained after citrate perfusion to calculate citrate-dependent steady-state currents. Conductance was calculated as the slope of linear fit to the *I–V* curves.

### Western blotting, co-immunoprecipitation, and biotinylation

Cell lysates were prepared by incubating the cells in an ice-cold lysis buffer containing 1× PBS, 10 mM $Na^+$ pyrophosphate, 50 mM NaF,1 mM $Na^+$ orthovanadate, 1% Triton X-100, and a mixture of protease inhibitors (Roche). For CoIP, extracts were incubated overnight with 1 $\mu$g/100 $\mu$l anti-$His_6$ tag mAb (Thermo Fisher Scientific), and the complexes were collected with either protein A– or G–Sepharose beads (Sigma–Aldrich) by incubation for 4 h at 4 °C. The beads were collected by centrifugation and washed three times with a lysis buffer, and the proteins were recovered by heating (37 °C for 30 min) in the SDS sample buffer. The samples were subjected to SDS-PAGE (8% gels) and subsequently transferred to nitrocellulose membranes (GE Whatman, Pittsburgh, PA). The membranes were probed with anti-tRFP (mKate) antibody (Evrogen, Moscow, Russia) diluted 1:3000. The membranes were then incubated with a secondary goat anti-rabbit IgG peroxidase conjugate antibody (Abcam), diluted at 1:10,000. To monitor human NaCT trafficking, we used a modified biotinylation assay as previously described (11). Briefly, transfected cells were washed and incubated with EZ-Link Sulfo-NHS-SS-Biotin (0.5 mg/ml; Thermo Fisher Scientific) for 30 min on ice. The biotin was quenched with 50 mM glycine, and lysates were prepared with the lysis buffer described above. Finally, 50 $\mu$l of a 1:1 slurry of immobilized neutravidin beads (Thermo Fisher Scientific) were added to 0.4 ml of cell extracts and incubated for 2 h at 4 °C. The beads were washed with a binding buffer, and proteins were released with 50 $\mu$l of SDS-loading buffer. The extracts were loaded onto 10% Tris-glycine SDS-PAGE gels, which were subsequently transferred onto a nitrocellulose membrane and probed with anti-NaCT mAb (Santa Cruz Biotechnology, Dallas, TX) diluted at 1:500. The membranes were then incubated with a secondary goat anti-mouse IgG peroxidase conjugate antibody (Thermo Fisher Scientific), diluted at 1:1,000. Densitometric analysis was performed using ImageJ software (21) for biotinylated and input immunoblot images (similar to the sample image presented in Fig. 3*E*). The ratio between the densitometry values (biotin/input) for each lane was averaged between independent experiments. The number of independent experiments (*N*) is indicated in the summary of Fig. 3*E*. $p > 0.05$ (not significant).

### Fluorescent microscopy

HEK293 cells were cultured on coverslips and transfected with either WT or mutant human NaCT. After 48 h the cells were fixed and washed with PBS. For immunofluorescence detection, the fixed cells were incubated with anti-NaCT mAb diluted 1:50 (Santa Cruz Biotechnology, Dallas, TX) for 60 min at room temperature. The cells were then washed three times in PBS and incubated with Cy3 goat anti-mouse IgG (H+L) (1:200; Jackson ImmunoResearch Laboratories) for 60 min at room temperature. The cells were washed three times in PBS, and the nuclei were stained with 4′,6′-diamino-2-phenylindole. The images were acquired using an Olympus BX60 microscope.

### Statistics

Significance was analyzed by Student's *t* test. The slopes of the *I–V* curves were calculated by linear regression statistics.

All results are presented as means ± S.E. *, $p < 0.05$; **, $p < 0.005$; and ***, $p < 0.0005$. *N* is represented in the summary figures as indicated in the figure or as the number of circles for each column.

*Author contributions*—A. K., S. A., H. E.-R., and E. O. data curation; A. K., S. A., H. E.-R., and E. O. formal analysis; A. K., S. A., H. E.-R., and E. O. methodology; A. K. and E. O. writing-original draft; E. O. conceptualization; E. O. resources; E. O. supervision; E. O. funding acquisition; E. O. validation; E. O. investigation; E. O. visualization; E. O. project administration; E. O. writing-review and editing.

## References


1. Markovich, D. (2012) Sodium-sulfate/carboxylate cotransporters (slc13). *Curr. Top. Membr.* **70,** 239–256 CrossRef Medline
2. Markovich, D., and Murer, H. (2004) The slc13 gene family of sodium sulphate/carboxylate cotransporters. *Pflugers Arch.* **447,** 594–602 CrossRef Medline
3. Pajor, A. M. (2014) Sodium-coupled dicarboxylate and citrate transporters from the slc13 family. *Pflugers Arch.* **466,** 119–130 CrossRef Medline
4. Prakash, S., Cooper, G., Singhi, S., and Saier, M. H., Jr. (2003) The ion transporter superfamily. *Biochim. Biophys. Acta* **1618,** 79–92 CrossRef Medline
5. Hardies, K., de Kovel, C. G., Weckhuysen, S., Asselbergh, B., Geuens, T., Deconinck, T., Azmi, A., May, P., Brilstra, E., Becker, F., Barisic, N., Craiu, D., Braun, K. P., Lal, D., Thiele, H., *et al.* (2015) Recessive mutations in SLC13A5 result in a loss of citrate transport and cause neonatal epilepsy, developmental delay and teeth hypoplasia. *Brain* **138,** 3238–3250 CrossRef Medline
6. Khamaysi, A., Anbtawee-Jomaa, S., Fremder, M., Eini-Rider, H., Shimshilashvili, L., Aharon, S., Aizenshtein, E., Shlomi, T., Noguchi, A., Springer, D., Moe, O. W., Shcheynikov, N., Muallem, S., and Ohana, E. (2019) Systemic succinate homeostasis and local succinate signaling affect blood pressure and modify risks for calcium oxalate lithogenesis. *J. Am. Soc. Nephrol.* CrossRef Medline
7. Ohana, E., Shcheynikov, N., Moe, O. W., and Muallem, S. (2013) slc26a6 and NaDC-1 transporters interact to regulate oxalate and citrate homeostasis. *J. Am. Soc. Nephrol.* **24,** 1617–1626 CrossRef Medline
8. Jiang, Z., Asplin, J. R., Evan, A. P., Rajendran, V. M., Velazquez, H., Nottoli, T. P., Binder, H. J., and Aronson, P. S. (2006) Calcium oxalate urolithiasis in mice lacking anion transporter Slc26a6. *Nat. Genet.* **38,** 474–478 CrossRef Medline
9. Rogina, B., Reenan, R. A., Nilsen, S. P., and Helfand, S. L. (2000) Extended life-span conferred by cotransporter gene mutations in *Drosophila*. *Science* **290,** 2137–2140 CrossRef Medline
10. Birkenfeld, A. L., Lee, H. Y., Guebre-Egziabher, F., Alves, T. C., Jurczak, M. J., Jornayvaz, F. R., Zhang, D., Hsiao, J. J., Martin-Montalvo, A., Fischer-Rosinsky, A., Spranger, J., Pfeiffer, A. F., Jordan, J., Fromm, M. F., König, J., *et al.* (2011) Deletion of the mammalian INDY homolog mimics aspects of dietary restriction and protects against adiposity and insulin resistance in mice. *Cell Metab.* **14,** 184–195 CrossRef Medline
11. Ohana, E., Shcheynikov, N., Yang, D., So, I., and Muallem, S. (2011) Determinants of coupled transport and uncoupled current by the electrogenic SLC26 transporters. *J. Gen. Physiol.* **137,** 239–251 CrossRef Medline
12. Mancusso, R., Gregorio, G. G., Liu, Q., and Wang, D. N. (2012) Structure and mechanism of a bacterial sodium-dependent dicarboxylate transporter. *Nature* **491,** 622–626 CrossRef Medline
13. Nie, R., Stark, S., Symersky, J., Kaplan, R. S., and Lu, M. (2017) Structure and function of the divalent anion/$Na^+$ symporter from *Vibrio cholerae* and a humanized variant. *Nat. Commun.* **8,** 15009 CrossRef Medline
14. Mulligan, C., Fenollar-Ferrer, C., Fitzgerald, G. A., Vergara-Jaque, A., Kaufmann, D., Li, Y., Forrest, L. R., and Mindell, J. A. (2016) The bacterial dicarboxylate transporter VcINDY uses a two-domain elevator-type mechanism. *Nat. Struct. Mol. Biol.* **23,** 256–263 CrossRef Medline
15. Mishra, V. K., Palgunachari, M. N., Segrest, J. P., and Anantharamaiah, G. M. (1994) Interactions of synthetic peptide analogs of the class A amphipathic helix with lipids: evidence for the snorkel hypothesis. *J. Biol. Chem.* **269,** 7185–7191 Medline
16. Schow, E. V., Freites, J. A., Cheng, P., Bernsel, A., von Heijne, G., White, S. H., and Tobias, D. J. (2011) Arginine in membranes: the connection between molecular dynamics simulations and translocon-mediated insertion experiments. *J. Membr. Biol.* **239,** 35–48 CrossRef Medline
17. Strandberg, E., and Killian, J. A. (2003) Snorkeling of lysine side chains in transmembrane helices: how easy can it get? *FEBS Lett.* **544,** 69–73 CrossRef Medline
18. Ashkenazy, H., Abadi, S., Martz, E., Chay, O., Mayrose, I., Pupko, T., and Ben-Tal, N. (2016) ConSurf 2016: an improved methodology to estimate and visualize evolutionary conservation in macromolecules. *Nucleic Acids Res.* **44,** W344–W350 CrossRef Medline
19. Hediger, M. A., Coady, M. J., Ikeda, T. S., and Wright, E. M. (1987) Expression cloning and cDNA sequencing of the Na+/glucose co-transporter. *Nature* **330,** 379–381 CrossRef Medline
20. Wright, E. M. (2013) Glucose transport families SLC5 and SLC50. *Mol. Aspects Med.* **34,** 183–196 CrossRef Medline
21. Schneider, C. A., Rasband, W. S., and Eliceiri, K. W. (2012) NIH Image to ImageJ: 25 years of image analysis. *Nat. Methods* **9,** 671–675 CrossRef Medline
22. Zwart, R., Peeva, P. M., Rong, J. X., and Sher, E. (2015) Electrophysiological characterization of human and mouse sodium-dependent citrate transporters (NaCT/SLC13A5) reveal species differences with respect to substrate sensitivity and cation dependence. *The J. Pharmacol. Exp. Ther.* **355,** 247–254 CrossRef Medline
23. Inoue, K., Zhuang, L., and Ganapathy, V. (2002) Human $Na^+$-coupled citrate transporter: primary structure, genomic organization, and transport function. *Biochem. Biophys. Res. Commun.* **299,** 465–471 CrossRef Medline
24. Kelly, B., and O'Neill, L. A. (2015) Metabolic reprogramming in macrophages and dendritic cells in innate immunity. *Cell Res.* **25,** 771–784 CrossRef Medline
25. Tannahill, G. M., Curtis, A. M., Adamik, J., Palsson-McDermott, E. M., McGettrick, A. F., Goel, G., Frezza, C., Bernard, N. J., Kelly, B., Foley, N. H., Zheng, L., Gardet, A., Tong, Z., Jany, S. S., Corr, S. C., *et al.* (2013) Succinate is an inflammatory signal that induces IL-1$\beta$ through HIF-1$\alpha$. *Nature* **496,** 238–242 CrossRef Medline
26. Söding, J., Biegert, A., and Lupas, A. N. (2005) The HHpred interactive server for protein homology detection and structure prediction. *Nucleic Acids Res.* **33,** W244–W248 CrossRef Medline
27. Newport, T. D., Sansom, M. S. P., and Stansfeld, P. J. (2019) The MemProtMD database: a resource for membrane-embedded protein structures and their lipid interactions. *Nucleic Acids Res.* **47,** D390–D397 CrossRef Medline
28. Pettersen, E. F., Goddard, T. D., Huang, C. C., Couch, G. S., Greenblatt, D. M., Meng, E. C., and Ferrin, T. E. (2004) UCSF Chimera: a visualization system for exploratory research and analysis. *J. Comput. Chem.* **25,** 1605–1612 CrossRef Medline
29. Madeira, F., Park, Y. M., Lee, J., Buso, N., Gur, T., Madhusoodanan, N., Basutkar, P., Tivey, A. R. N., Potter, S. C., Finn, R. D., and Lopez, R. (2019) The EMBL-EBI search and sequence analysis tools APIs in 2019. *Nucleic Acids Res.* **47,** W636–W641 CrossRef Medline
30. Shcheynikov, N., Kim, K. H., Kim, K. M., Dorwart, M. R., Ko, S. B., Goto, H., Naruse, S., Thomas, P. J., and Muallem, S. (2004) Dynamic control of cystic fibrosis transmembrane conductance regulator $Cl^-/HCO_3^-$ selectivity by external $Cl^-$. *J. Biol. Chem.* **279,** 21857–21865 CrossRef Medline